Chinese Chemical Letters 36 (2025) 110166

Contents lists available at ScienceDirect

Chinese Chemical Letters

journal homepage: www.elsevier.com/locate/cclet

Two-dimensional design strategy to construct smart dual-responsive fluorescent probe for the precise tracking of ischemic stroke

Jiayu Zeng[a,b,c,1], Minhui Liu[a,b,1], Ting Yang[a,b], Jia Huang[a], Songjiao Li[a,b], Wanting Zhang[a], Dan Cheng[b,c,d,*], Longwei He[a,b,c,*], Jia Zhou[a,*]

[a] Department of Ultrasound Medicine, The First Affiliated Hospital, Hengyang Medical School, University of South China, Hengyang 421002, China
[b] MOE Key Lab of Rare Pediatric Diseases, School of Pharmaceutical Science, Hengyang Medical School, University of South China, Hengyang 421002, China
[c] School of Basic Medical Science, Hengyang Medical School, University of South China, Hengyang 421001, China
[d] Department of Gastroenterology, Clinical Research Institute, The Affiliated Nanhua Hospital, Hengyang Medical School, University of South China, Hengyang 421002, China

ARTICLE INFO

Article history:
Received 24 April 2024
Revised 19 June 2024
Accepted 21 June 2024
Available online 22 June 2024

Keywords:
Ischemic stroke
Ferroptosis
Viscosity
Cysteine
Mitochondria
Fluorescent probe

ABSTRACT

Early recognition is key to improving the prognosis of ischemic stroke (IS), while available imaging methods tend to target events that have already undergone ischemia. A new method to detect early IS is urgently needed, as well as further study of its mechanisms. Viscosity and cysteine (Cys) levels of mitochondria have been associated with ferroptosis and IS. It is possible to identify IS and ferroptosis accurately and early by monitoring changes in mitochondrial Cys and viscosity simultaneously. In this work, a viscosity/Cys dual-responsive mitochondrial-targeted near-infrared (NIR) fluorescent probe (**NVCP**) was constructed for the precise tracking of IS using a two-dimensional design strategy. **NVCP** consists of a chromophore dyad containing diethylaminostyrene quinolinium rotor and chloro–sulfonylbenzoxadiazole (SBD-Cl) derivative with two easily distinguished emission bands (λ_{em} = 592 and 670 nm). **NVCP** performs the way of killing two birds with one stone, that is, the probe exhibits excellent selectivity and sensitivity for detecting viscosity and Cys in living cells with excellent biocompatibility and accurate mitochondrial targeting capability by dual channel imaging mode. In addition, **NVCP** recognized that the viscosity increases and Cys level decreases in cells when undergoing ferroptosis and oxygen-glucose deprivation (OGD) stress by confocal imaging, flow cytometry, and Western blot experiments. Treatment of ferroptosis inhibitors (ferrostatin-1 (Fer-1) and deferoxamine (DFO)) could reverse the variation tendency of viscosity and Cys. This is the first time that the relationship between ferroptosis and IS was identified through an analysis of Cys and viscosity. More importantly, the ischemic area was also instantly distinguished from normal tissues through fluorescence imaging of **NVCP** *in vivo*. The developed NIR dual-responsive probe **NVCP** toward viscosity and Cys could serve as a sensitive and reliable tool for tracking ferroptosis-related pathological processes during IS.

Ischemic stroke (IS), characterized by local ischemia and hypoxia of the brain that causes disability and 9% of all deaths around the world, has become an important public health problem as the global population ages with one in four people affected over their lifetime [1,2]. Despite the management of IS has greatly advanced, the addition of computed tomography (CT) perfusion imaging and angiography allows a positive diagnosis of IS, IS patients have an early mortality rate of 10%–12% higher than the general population [2,3].

Current available imaging methods tend to target events that have already undergone ischemia rather than identifying IS at an early stage. Early recognition is key to improving the prognosis and timely intervention of IS, which requires a deeper understanding of its mechanism [4]. Ferroptosis, identified as iron-reliant programmed cell demise, exhibits lipid peroxidation and mitochondrial shrinkage [5] and has been linked to neurological diseases, including neurodegenerative disease [6], cancer [7], epilepsy [8], and ischemic stroke [9]. Studies have shown that ferroptosis could contribute heavily to IS occurrence and development, and inhibiting ferroptosis can improve IS outcomes [10-13]. However, there are few details about how ferroptosis operates in early IS.

Cysteine (Cys), a crucial thioalcohol in maintaining redox balance, participates in energy generation and transmission through

* Corresponding authors.
E-mail addresses: flychand0110@163.com (D. Cheng), helongwei0110@163.com (L. He), jiazhou.dr@foxmail.com (J. Zhou).
[1] These authors contributed equally to this work.

https://doi.org/10.1016/j.cclet.2024.110166
1001-8417/

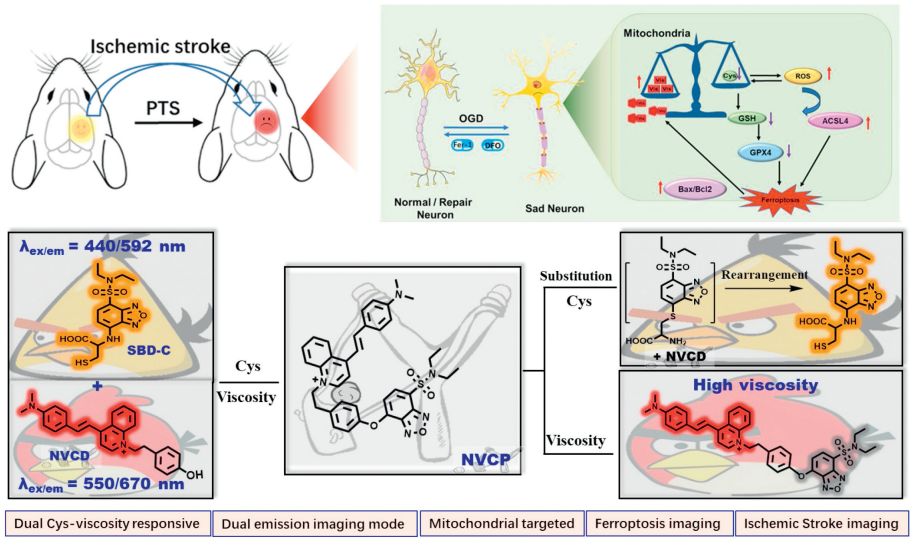

Scheme 1. The proposed mechanism of probe **NVCP** for monitoring ferroptosis during IS by response with viscosity and Cys.

chemical reactions such as fatty acid oxidation, amino acid decomposition, aerobic metabolism, and phosphorylation in mitochondria, which is closely related to IS and ferroptosis [14-17]. A sharply reduced Cys level can be found in the brain due to an explosion of reactive oxygen species in the early stages of IS [17]. Researchers also found that *N*-acetyl-L-cysteine (NAC, a Cys derivative), an antioxidant drug commonly used in clinical treatment, has the potential as a thrombolytic drug for the treatment of IS [18,19]. Additionally, Cys deprivation can lead to a decrease in glutathione (GSH) and GSH peroxidase 4 (GPX4) levels, further leading to the accumulation of glutamate, rendering cells more susceptible to ferroptosis [16,20]. These shreds of evidence indicated that Cys plays an important role in ferroptosis and IS. The development of reactive imaging tools that monitor the dynamic changes of Cys in mitochondria is conducive to the research of ferroptosis during IS.

Viscosity is a major determinant of the flow state of the microenvironment, encompassing lipids, proteins, and polysaccharides, and is essential for signal transmission and microbial interaction within cells [21-24]. Abnormal viscosity is intricately linked to a range of diseases, including Alzheimer's disease (AD) [22], diabetes [25], cancers [26], and IS [27]. Blood viscosity is elevated during acute and chronic periods of IS, and cases of IS are more likely to occur in people with high blood viscosity [28,29]. In mitochondria, abnormal viscosity inhibits the electron transport chain activity and leads to dysfunction of the mitochondrial function which is followed by apoptosis [14], autophagy [30], and ferroptosis [31-34]. Therefore, monitoring the changes of viscosity in mitochondria *in situ* is also highly significant for comprehending the role of ferroptosis and unraveling the mechanisms underlying the development of IS.

Fluorescence imaging technology takes the advantages of simple operation, low cost, good selectivity, and real-time *in situ* analysis, and has become an indispensable detection method in biomedical research [35-38]. So far, a series of fluorescence probes for IS imaging have been developed. The response indicators of these fluorescent probes are mainly pH [39], thiol reductase [40-42], metalloproteinases [43], nitric oxide [44], peroxynitrite ions [45], Fe^{2+} [46], H_2S [47], and viscosity [27,31-34]. Despite these probes being useful for detecting pathological changes in IS cells and organism, most are restricted to detecting only a single active bioindicator, which makes it difficult to address complex biological demands [48]. Monitoring disease progress can be improved by real-time synchronous imaging of multiple biomarkers. To this end, this work aims to design and synthesize a mitochondrial-targeted near-infrared fluorescence probe (**NVCP**) with dual viscosity/Cys-specific response for *in situ* tracing the spatiotemporal distribution of viscosity and Cys during ferroptosis and IS. **NVCP** contains two important moieties, the viscosity response reporter and the Cys response reporter (Scheme 1), and the positively charged quinolinium promotes the probe to anchor in mitochondria. **NVCP** could achieve *in situ* imaging tracing of mitochondrial viscosity and Cys during ferroptosis and provide a reliable visualization tool for recognizing and researching IS early. To achieve simultaneous and accurate detection of mitochondrial viscosity and Cys, a near-infrared (NIR) emissive and positively charged rotor diethylaminostyrene quinolinium and a Cys-specific sulfonylbenzoxadiazole (SBD) chromophore were chosen to construct the fluorescent probe dyad (**NVCP**) with two distinguishable response emission bands (Scheme 1). The molecular rotor is condensed from 4-methylquinoline quaternary ammonium salt and *N*,*N*-dimethylamino benzaldehyde, forming a typical D-π-A system. Under low viscosity conditions, the fluorescence of the rotor would be quenched due to the non-radiative transition caused by the rotation of internal bonds. However, in high-viscosity states, the internal rotation limitation leads to an enhanced fluorescence at the NIR region (670 nm) with a large Stoke shift (120 nm). At the same time, chloro–sulfonylbenzoxadiazole (SBD-Cl) was introduced as a Cys-specific recognition fluorophore. In the presence of Cys, **NVCP** is first cleaved through nucleophilic substitution, then followed by intramolecular rearrangement to form amino substituted derivatives and emitted orange fluorescence (592 nm). In addition, the positive charge of the probe is beneficial for anchoring in mitochondria. **NVCP** was synthesized by routine in Scheme S1 (Supporting information).

With **NVCP** in hand, the response of **NVCP** for Cys was investigated using absorption and emission spectroscopic measurements. All absorption and fluorescence spectra tests were performed in phosphate buffer (25 mmol/L, pH 7.4, 30% *N*,*N*-dimethylformamide (DMF)). For absorption spectra, **NVCP** displayed the maximum absorption peak centered at 550 nm, while the peak increased slightly and accompanied with generation of an absorption shoulder band centered at about 440 nm after incubation with Cys (Fig. 1A). In emission response spectra, a strong emission band centered at 592 nm was generated upon the addition of Cys and reached a plateau (63-fold enhancement) after 70 min (Fig. 1B and Fig. S1 in Supporting information). A direct linear relationship

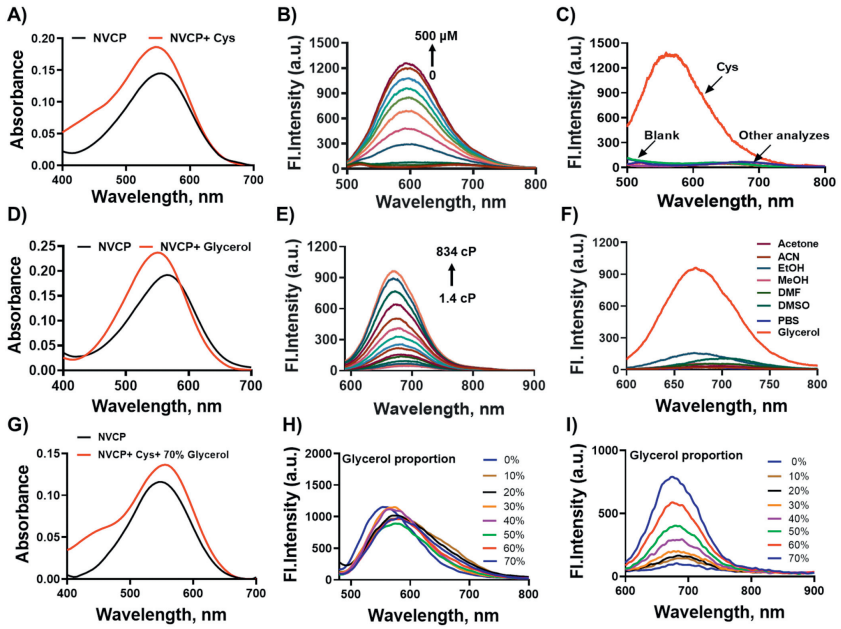

Fig. 1. (A) Absorption of **NVCP** (10 μmol/L) before and after the addition of Cys. (B) Fluorescence titration of **NVCP** to different concentrations of Cys (0–500 μmol/L). (C) Fluorescence response of **NVCP** to Cys and other analytes (H_2S, GSH, Hcy, K^+, Ca^{2+}, Mg^{2+}, DL-lysine, DL-proline, DL–serine, D-phenylalanine, L-alanine, L-glutamine, L-arginine, L-leucine, L-threonine, L-valine, L-histidine, Glycine 100 μmol/L, respectively). The above data were recorded in a PBS solution (10 mmol/L, pH 7.4, 30% DMF), λ_{ex} = 440 nm. (D) Absorption spectra of **NVCP** in buffer and glycerol. (E) Fluorescence spectra of **NVCP** in buffer-glycerol mixtures with different viscosities. (F) Fluorescence response of **NVCP** to different solvents, λ_{ex} = 550 nm. (G) Absorption spectra of **NVCP** (10 μmol/L) in the absence or presence of Cys (500 μmol/L) and glycerol (70% volume ratio) in DMF. Fluorescence response spectra of **NVCP** to viscosity in the presence of Cys (500 μmol/L) with an excitation at 440 nm (H) or 550 nm (I) in DMF containing different proportions of glycerol.

ranging from 0 to 400 μmol/L was shown (Fig. S2 in Supporting information) and the detection limit was 37 μmol/L. Importantly, the fluorescence intensity of **NVCP** did not appear any change when treated with other bioactive agents, while Cys triggered a clear fluorescence enhancement at 592 nm (Fig. 1C and Fig. S3 in Supporting information), indicating that the response of the **NVCP** to Cys cannot be disturbed by these bioactive analytes. Fig. S4 (Supporting information) showed a strong fluorescence within the pH range of 7–10, indicating the probe's detection availability in organism. These results collectively indicated that **NVCP** could be applied in selectively monitoring the changes of Cys in biological samples.

Next, to verify the reliability of probe **NVCP** responding to viscosity, the optical performance in a phosphate buffer saline (PBS)-glycerol system was firstly investigated. As displayed in Fig. 1D, a maximum absorption peak at 550 nm was observed from **NVCP** in buffer, while the absorption was enhanced with a slight blue-shift after incubation with glycerol. In emission response spectra, **NVCP** exhibited a 22-fold fluorescence enhancement upon a viscosity change from 1.4 cP to 834 cP at 670 nm (Fig. 1E). A direct linear relationship from a plot of Log I_{670nm} against Logη ranging from 0.5 to 2.0 was also found (Fig. S5 in Supporting information). Meanwhile, the fluorescence emission of **NVCP** response with viscosity was hardly disturbed by biological analytes (Fig. S6 in Supporting information) and rarely depended on pH (Fig. S7 in Supporting information). The absorption and fluorescence spectra of **NVCP** in some solvents with different polarities were measured as polarity may influence molecular rotors' ability to detect viscosity. The absorption wavelength of **NVCP** in different polarities solvents hardly changed (Fig. S8 in Supporting information). No obvious fluorescence changes were also observed at 670 nm in different polar solutions with **NVCP** while a significant emission was generated in glycerol (Fig. 1F), which demonstrated that viscosity detection with **NVCP** is not hindered by the polarity of environment.

To evaluate the response performance of probe simultaneously towards Cys and viscosity, the fluorescence spectra were recorded at different viscosity in the presence of excess of Cys (500 μmol/L). A new absorption shoulder band centered at about 440 nm was also generated in response spectra (Fig. 1G). In addition, the response of **NVCP** to Cys was unaffected by the increased viscosity with an excitation at 440 nm (Fig. 1H), meanwhile, **NVCP** exhibited an obvious turn-on fluorescence response to viscosity in the presence of excess Cys when excited at 550 nm (Fig. 1I), which was almost equal with the change trends of response fluorescence of the rotor dye **NVCD** towards viscosity (Fig. S9 in Supporting information). Results from the above study demonstrated that **NVCP** could be used for detecting changes in Cys and viscosity simultaneously in a sensitive and specific manner in biological system.

To investigate whether there exists a fluorescence resonance energy transfer (FRET) process on molecule **NVCP**, we supplemented the fluorescence spectrum of **NVCP** with an excitation at SBD moiety (440 nm) and rotor **NVCD** (550 nm), respectively. As shown in Fig. S10 (Supporting information), negligible fluorescence was observed when excited at potential energy donor, while strong fluorescence was generated when excited at potential energy acceptor, suggesting the excited energy of SBD moiety cannot accepted by rotor molecule **NVCD**. The results indicated that there exists no FRET process on probe **NVCP**.

Prior to cell imaging, the methylthiazolyldiphenyl-tetrazolium bromide (MTT) study was performed to test **NVCP** cytotoxicity in PC12 cells. As shown in Fig. S11 (Supporting information), **NVCP** presented more than 90% of cells survived when **NVCP** (0–20 μmol/L) was incubated with PC12 cells for 24 h, indicating its suitability for live cell imaging. Then the intracellular location of **NVCP** was characterized using a confocal laser microscope with Mito-tracker green and lyso-tracker green. As shown in Fig. 2, **NVCP**'s red channel fluorescence image and Mito-tracker green's green channel fluorescence image overlapped significantly at a high Pearson coefficient (0.94). Close synchronization of intensity profiles was also observed between **NVCP** and Mito-tracker green-stained linear regions of interest (ROIs). However, the green chan-

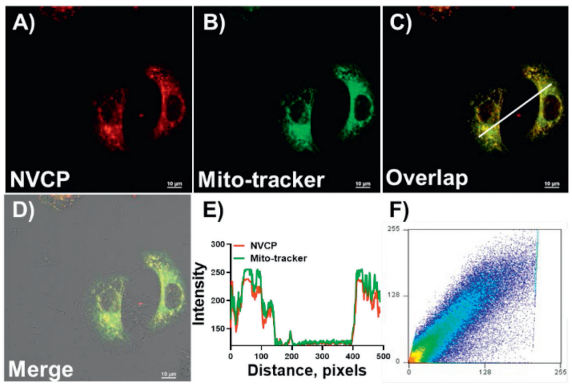

Fig. 2. Confocal laser fluorescence microscopic images of PC12 cells treated with **NVCP** and Mito-tracker green. (A) Red fluorescence image of **NVCP** ($\lambda_{ex}/\lambda_{em}$: 594/640–710 nm). (B) Green fluorescence image of Mito-tracker green ($\lambda_{ex}/\lambda_{em}$: 488/500–520 nm). (C) Overlap image of (A) and (B). (D) Merge of (C) and bright field. Scale bar: 10 μm. (E) Intensity profile of ROI across PC12 cells. (F) Correlation plot of Mito-tracker green and **NVCP** intensities.

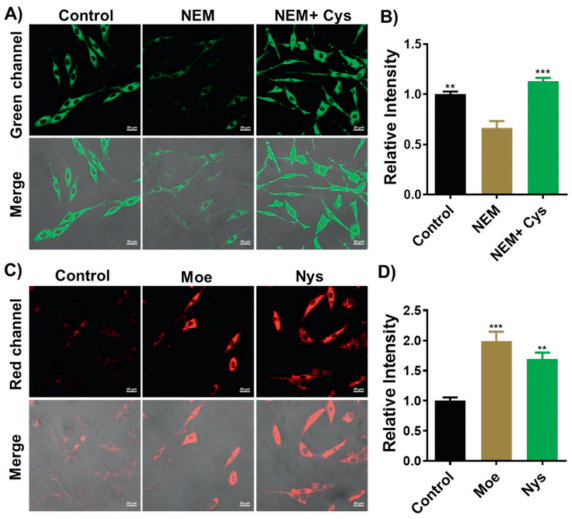

Fig. 3. (A) Confocal imaging of exogenous and endogenous Cys in PC12 cells with **NVCP**. Control group, cells were only loaded with **NVCP** for 30 min. NEM group, cells pretreated with NEM (200 μmol/L) for 30 min before being loaded with **NVCP**. NEM + Cys group, cells were treated with NEM (200 μmol/L) for 30 min, followed by an extra Cys (100 μmol/L) for 30 min incubation, $\lambda_{ex}/\lambda_{em}$ = 488 nm/540–600 nm. (B) Relative fluorescence intensity of images in (A). $^{**}P < 0.01$, $^{**}P < 0.001$. *vs.* NEM group. (C) Confocal laser fluorescence imaging of **NVCP** in PC12 cells pretreated with or without 10 μmol/L Moe and 10 μmol/L Nys for 30 min, then incubated with **NVCP** for 30 min, $\lambda_{ex}/\lambda_{em}$ = 594 nm/640–710 nm. Scale bar: 20 μm. (D) Relative fluorescence intensity of images in (C). $^{**}P < 0.01$, $^{**}P < 0.001$. *vs.* control group. Data are presented as mean ± standard deviation (SD) ($n = 3$).

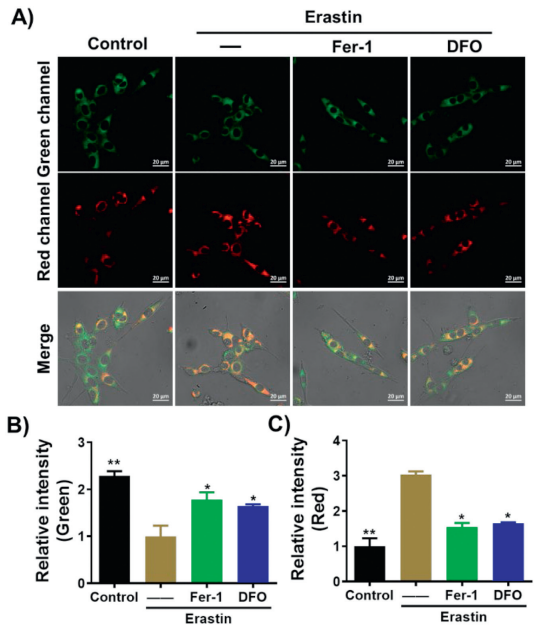

Fig. 4. (A) Confocal laser fluorescence imaging of **NVCP** in ferroptosis. (A) PC12 cells were stimulated with erastin (20 μmol/L, 30 min) before incubation with **NVCP** (10 μmol/L, 30 min), with or without pretreated with Fer-1 (20 μmol/L, 1 h) and DFO (100 μmol/L, 1 h). Cells only loaded with **NVCP** as the control group. Scale bar: 20 μm. (B, C) Relative fluorescence intensities of images in green and red channels for Cys ($\lambda_{ex}/\lambda_{em}$ = 488 nm/540–600 nm) and viscosity ($\lambda_{ex}/\lambda_{em}$ = 594 nm/640–710 nm), respectively. $^{*}P < 0.05$, $^{**}P < 0.01$ *vs.* erastin group. Data are presented as mean ± SD ($n = 3$).

nel fluorescence image of lyso-tracker green and red channel fluorescence image of **NVCP** less overlapped with a low Pearson's coefficient (0.23) (Fig. S12 in Supporting information). These data demonstrated **NVCP** accumulated in mitochondria with low cytotoxicity. The lipophilicity testing of probe **NVCP** has been also conducted. **NVCP** exhibits significant absorption in the octanol layer, while the water layer is relatively low (Fig. S13 in Supporting information), and the Log*P* value (one key consideration for crossing blood-brain barrier (BBB) for small molecules) of **NVCP** was calculated to be 1.59, indicating that **NVCP** has good lipophilicity and favourable BBB penetration ability.

Next, we evaluated the potential ability of **NVCP** for fluorescence imaging of Cys in living cells. As shown in Fig. 3A, PC12 cells were only incubated with **NVCP** and exhibited a fluorescence signal at the green channel. By comparison, the cells pretreated with *N*-ethylmaleimide (NEM, thiols-blocking agent) [49,50] showed significantly lower green fluorescence signals, which implied that **NVCP** was surely sensitive to the change of intracellular Cys. Moreover, the cells with additional Cys have observed notably stronger fluorescence intensity than cells in the NEM group (Fig. 3B). These results illustrated the sensitivity of **NVCP** to detect exogenous/endogenous Cys in living cells, indicating that **NVCP** has great potential for bioimaging Cys.

Furthermore, to validate the capability of **NVCP** for imaging mitochondrial viscosity, fluorescence images of PC12 cells were acquired in the presence of viscosity inducers. As shown in Figs. 3C and D, cells pretreated with monensin (Moe) or nystatin (Nys) displayed a stronger red fluorescence signal than cells in the control group loaded only with **NVCP**, indicating that the viscosity of mitochondria increased after Moe and Nys stimulation, which is consistent with the literature report [21,51]. These above results indicated that **NVCP** could be used to monitor the mitochondrial viscosity and Cys changes in the living system.

Recent studies have shown that Cys deprivation and abnormal viscosity are the key aspects of ferroptosis [20,52]. In this process, **NVCP** was used to monitor the changes of Cys and viscosity in living cells to demonstrate **NVCP**'s universality as a non-invasive tool to evaluate ferroptosis. Erastin (ferroptosis inducer) [53] was applied to PC12 cells in the ferroptosis group and pre-treated with ferrostatin-1 (Fer-1) [54] and deferoxamine (DFO) [55] before inducing ferroptosis in the ferroptosis inhibition group. All groups were incubated with **NVCP**, and the cells were only loaded with **NVCP** as a control group. As shown in Fig. 4A, the cells of the ferroptosis group showed weakened fluorescence in the green channel and enhanced fluorescence in the red channel when compared to that of the control group, respectively, indicating that Erastin induced a decrease in Cys and an increase in viscosity in PC12 cells. Meanwhile, both Fer-1 and DFO reversed fluorescence changes in the green and red channels when compared with the Erastin group

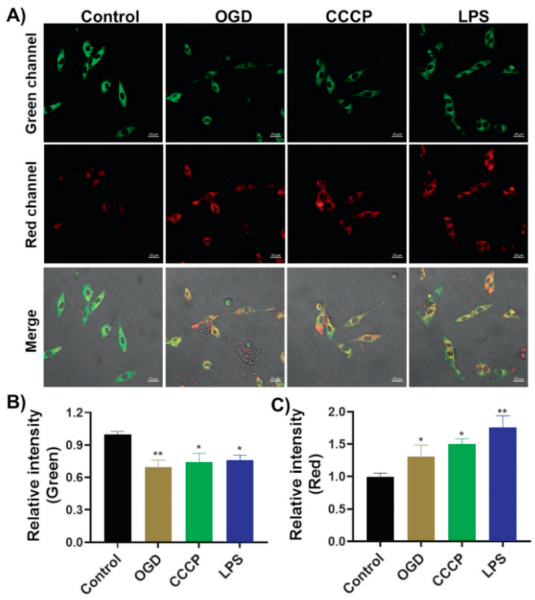

Fig. 5. (A) Confocal laser fluorescence images of PC12 cells during an ischemic environment. Cells in the control group were incubated with **NVCP** only for 30 min, cells in the OGD group suffered from oxygen and glucose deprivation for 2 h, and cells in the CCCP group and LPS group were incubated with CCCP (1 μmol/L) or LPS (5 μg/mL) for 30 min and then loaded **NVCP**, green channel for Cys ($\lambda_{ex}/\lambda_{em}$ = 488 nm/540–600 nm), and red channel for viscosity ($\lambda_{ex}/\lambda_{em}$ = 594 nm/640–710 nm). Scale bar: 20 μm. (B) Relative fluorescence intensity in green channel of images in (A). (C) Relative fluorescence intensity in red channel of images in (A). $^{*}P < 0.05$, $^{**}P < 0.01$ *vs.* control group. Data are presented as mean ± SD ($n = 3$).

(Figs. 4B and C). These results indicated that **NVCP** could visualize ferroptosis by Cys and viscosity changes in mitochondria.

Mitochondrial viscosity and Cys also have been proven to be important markers of IS [15-20]. Next, we also examined **NVCP** as a method of detecting viscosity and Cys levels during IS in PC12 cells. Oxygen and glucose deprivation (OGD), Carbonyl cyanide 3-chlorophenylhydrazone (CCCP), and lipopolysaccharide (LPS) were chosen to stimulate PC12 cells to mimic the microenvironment of IS in neuron cells [56-58]. As shown in Fig. 5A, OGD-treated cells caused remarkably weaker fluorescence intensity in the green channel and stronger fluorescence intensity in the red channel than cells only loaded with **NVCP** respectively, which meant that a reduction of Cys was accompanied by an increase in viscosity during ischemic microenvironments. To imitate the complex microenvironment of IS in multiple aspects, CCCP was employed to induce mitochondrial stress conditions. CCCP can lead to viscosity variation and GSH depletion of the intracellular microenvironment due to inducing disruption of mitochondrial membrane potential and selectively increasing the permeability of lipid membranes to protons [59]. As expected, the faded fluorescence in the green channel and increased fluorescence in the red channel were observed in the CCCP group. In addition, the commonly oxidative stress inducer LPS was also used to mimic the oxidative stress microenvironment during IS [60,61]. The fluorescence imaging results were consistent with those of the OGD group and CCCP group (Figs. 5B and C). These results indicated that **NVCP** can be well applied to monitor the mitochondrial viscosity and Cys changes in IS-related microenvironment.

Encouraged by the above imaging experiments, it is reasonable to believe that monitoring the changes of Cys and viscosity in mitochondria could help explain the relationship between ferroptosis and IS. Subsequently, we examined the association between ferroptosis and OGD cells by **NVCP** (Fig. 6A). As shown in Fig. 6B, the OGD group showed weaker fluorescence intensity in the Cys channel and stronger fluorescence intensity in the viscosity channel when compared with the control group. However, both Fer-1 and DFO reversed the phenomenon (Figs. 6C and D), indicating that ferroptosis variation is primarily responsible for the fluorescence signal changes during OGD. To further validate this result, we used flow cytometry to detect the fluorescence intensity changes of

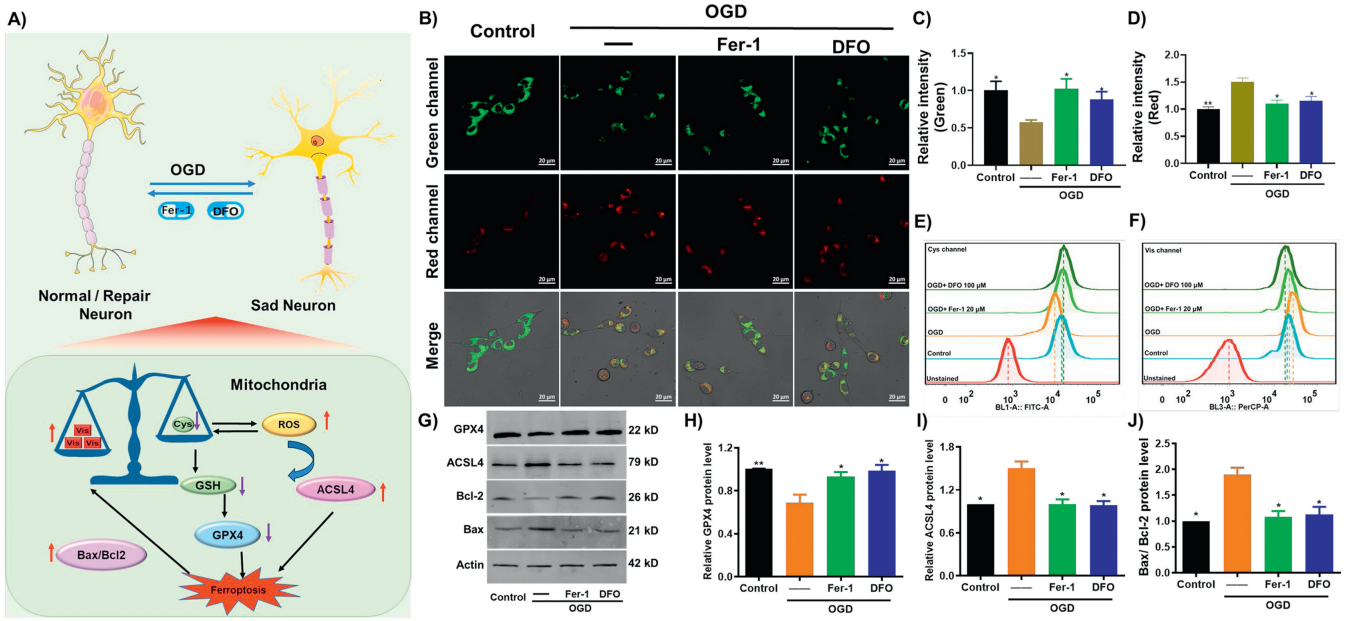

Fig. 6. (A) The possible mechanism of ferroptosis in OGD-induced ischemic stroke injury. (B) Confocal laser fluorescence imaging of **NVCP**-loaded PC12 cells. PC12 cells were cultured with OGD (2 h) followed by loading with **NVCP** (10 μmol/L, 30 min), with or without pretreated with Fer-1 (20 μmol/L, 1 h) and DFO (100 μmol/L, 1 h). Cells only loaded with **NVCP** as control. Scale bar: 20 μm. (C, D) Relative fluorescence intensities of images in green and red channels for Cys ($\lambda_{ex}/\lambda_{em}$ = 488 nm/540–600 nm, C) and viscosity ($\lambda_{ex}/\lambda_{em}$ = 594 nm/640–710 nm, D), respectively. (E, F) Flow cytometry analysis of panel (B) in fluorescein isothiocyanate (FITC) (E) and PerCP (F) channel for Cys and viscosity, respectively. (G) Western blot illustrating the expression of GPX4, ACSL4, Bax, and Bcl-2 in the PC12 cells of panel (B), actin was used as a loading control. Quantitative data of Western blot results for GPX4 (H), ACSL4 (I), and Bax/Bcl-2. (J) were normalized by ImageJ software. $^{*}P < 0.05$, $^{**}P < 0.01$ *vs.* OGD group. Data are presented as mean ± SD ($n = 3$).

the Cys channel and viscosity channel in each group of cells with **NVCP** (Figs. 6E and F), which was consistent with imaging results. These results confirmed that **NVCP** has the capability to track the dynamic changes of Cys and viscosity during the IS process and its ferroptosis inhibition.

Previous studies revealed that the deprivation of Cys inhibited the expression of GPX4 and excessive lipid peroxidation, triggers the process of ferroptosis [14,15]. IS cells and mice exhibited reduced Cys/GPX4 levels and increased acyl-CoA synthetase long-chain family member 4 (ACSL4) expression and lipid peroxidation [11,62,63]. GPX4 can inhibit excessive lipid peroxidation in neurons, and its inhibition or knockout trigger ferroptosis [7,62]. ACSL4 [11], a crucial variant for the metabolism of polyunsaturated fatty acids, plays a significant role in determining the susceptibility to ferroptosis by increasing lipid peroxidation (Fig. 6A).

Thus, we further determined the levels of GPX4 and ACSL4 by Western blot in the process of IS involving ferroptosis (Fig. 6G). Our results showed that the expression levels of GPX4 were considerably downregulated in the OGD group, and it was further upregulated by the treatment with Fer-1 and DFO (Fig. 6H). Meanwhile, the expression levels of ACSL4 were significantly higher in the OGD group than that of the control group and further downregulated by the treatment of Fer-1 and DFO (Fig. 6I). In addition, we evaluated the levels of Bax and Bcl-2, two proteins associated with the outcome of ferroptosis. The Bcl-2 gene family contains the apoptosis-promoting Bax, which antagonizes Bcl-2′s benefits and leads to cell death [6]. As shown in Fig. 6J, the upregulation of Bax/Bcl-2 was followed by OGD in living cells, and they were reversed by the treatment of Fer-1 and DFO. These data indicated that the interventions of ferroptosis can repair cell damage caused by OGD to some extent. Taken together, these results demonstrate that **NVCP** can be used to monitor mitochondrial Cys and viscosity during ferroptosis-related OGD.

Motivated by the above series of imaging results in PC12 cells, we further explored the ability of **NVCP** for imaging IS *in vivo* by detection of viscosity-responding NIR fluorescence signal. All experiments using mice were approved by Medical Ethics Committee, University of South China and operated in accordance with University of South China guidelines on the care and use of animals for scientific purposes. Before *in vivo* imaging, hematoxylin and eosin (H&E) staining and some blood biochemical indexes was performed to test the biocompatibility of **NVCP** *in vivo* (Fig. S14 in Supporting information). In addition, no noticeable difference in organs was observed *via* H&E stains. Even at a concentration of 20 μmol/L, **NVCP** did not cause hemolysis, which indicated that **NVCP** is suitable for imaging analysis of mice *in situ* (Fig. S15 in Supporting information). A mice model of photothrombotic ischemia stroke (PTS) was selected to produce a mice model suffering from IS [64].

The actual fabrication of the PTS model and imaging was accomplished as depicted in the experimental setup. As shown in Fig. S16 (Supporting information), the fluorescence intensity of the ischemic site in the PTS group increased significantly compared to that of the sham group, probably resulting from the abnormal increase of viscosity after disruption during IS, indicating **NVCP** can recognize ischemic sites. Moreover, we also evaluated the location and extent of the ischemia by stereotaxic injection of **NVCP**. The NIR fluorescence intensity of the ischemic site (laser irradiated site) in the PTS group was significantly enhanced compared with the sham group only loaded with **NVCP** for up to 120 min (Fig. S16A). Stripping the brain tissue of mice also yielded consistent results with detection *in vivo*, and no significant fluorescence was observed in other major organs (Fig. S16B and C). Furthermore, the fluorescence of the ischemic location gradually increased after tail vein injection with **NVCP** reaching the maximum at 20 min and maintaining it for about 60 min (Fig. S17 in Supporting information). These results proved that **NVCP** was suitable for *in situ* IS imaging.

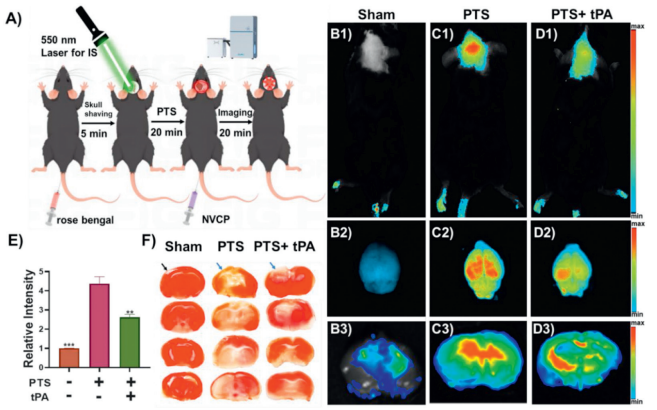

Fig. 7. (A) Schematic illustration of the IS model and probe treatment operation. NIR fluorescence imaging of **NVCP** tail vein injected during IS *in vivo* (B1–D1), brain tissue (B2–D2), and coronal brain slices (B3–D3), $\lambda_{ex}/\lambda_{em} = 640\,nm/695\,nm$. (E) Relative fluorescence intensity of images in (B1–D1). $^{**}P < 0.01$, $^{***}P < 0.001$ *vs.* sham group. Data are presented as mean ± SD ($n = 3$). (F) Images of TTC-stained coronal brain sections, ischemic tissue appears as white color, the quantitative analysis of infarct volume% was shown in Fig. S19.

For patients with IS, timely restoration of blood flow is the most important therapeutic goal, t-PA has been the most commonly used thrombolytic drug in first-line treatment for IS clinical [65,66]. Therefore, we carried out the experiment of IS by treating with t-PA within 2 h after PTS and examined the responses of **NVCP** to the changes in ischemic range after treatment. The IS mice model and probe treatment operation was illustrated in Fig. 7A. As expected, a significant decrease in fluorescence intensity and area was detected in mice treated with t-PA compared with the PTS group (Fig. 7D), indicating that t-PA restores some blood supply to the IS's brain, and this process can be monitored *in situ* by the NIR fluorescence imaging of **NVCP** (Fig. 7E). Moreover, organ and slice fluorescence imaging *in vitro* also confirm the above results (Figs. 7B–D and Fig. S18 in Supporting information). Additionally, 2,3,5-triphenyltetrazolium chloride (TTC) staining was also used to confirm the ischemic area by infarct size after 24 h TTC stains normal tissue a deep red color while ischemic tissue unstained by TTC appears a white color. As shown in Fig. 7F and Fig. S19 (Supporting information), the brain slices in the PTS model showed a remarkable infarct volume compared with that of the Sham group. The TTC-unstained infarcted area in tPA-treated mice was smaller than that of the PTS model mice at 24 h of recovery, which high agreement with **NVCP** fluorescence imaging *in vivo* and *in vitro*. These above results suggested that **NVCP** possesses great potential for early *in situ* recognizing and monitoring of the changes in ischemic area during IS.

In conclusion, a viscosity/Cys dual-responsive mitochondrial-targeted fluorescent probe (**NVCP**) was reasonably developed for precisely tracking IS using a two-dimensional design strategy. **NVCP** performs the way of killing two birds with one stone, that is, the chromophore dyad-based probe exhibits excellent selectivity and sensitivity for detecting viscosity and Cys in living cells with excellent biocompatibility and accurate mitochondrial targeting capability by dual channel imaging mode ($\lambda_{em} = 592$ and 670 nm). The dynamic changes of viscosity increase and Cys decrease as well as the reversal tendency after treatment of ferroptosis inhibitors (Fer-1 and DFO) in the ferroptosis process and IS microenvironment were monitored successfully with the help of **NVCP**. What's more, **NVCP** was applied as a visual tool to track the *in situ* viscosity ischemia area during IS and its treatment in PTS model mice, which was in high agreement with pathological morphology stain-

ing. This is the first time that the relationship between ferroptosis and IS was identified through an analysis of Cys and viscosity. The results above suggested that **NVCP** could potentially serve as a reliable and noninvasive visual measurement tool for studying ferroptosis and ferroptosis-related events, such as IS.

Declaration of competing interest

The authors declare that they have no known competing financial interests or personal relationships that could have appeared to influence the work reported in this paper.

CRediT authorship contribution statement

Jiayu Zeng: Writing – original draft, Methodology, Investigation, Formal analysis, Data curation, Conceptualization. **Minhui Liu:** Methodology, Investigation, Data curation. **Ting Yang:** Methodology, Investigation, Formal analysis, Data curation. **Jia Huang:** Software, Methodology, Investigation, Formal analysis, Data curation. **Songjiao Li:** Methodology, Investigation, Formal analysis, Data curation. **Wanting Zhang:** Methodology, Investigation, Formal analysis, Data curation. **Dan Cheng:** Writing – review & editing, Supervision, Resources, Project administration, Methodology, Investigation, Funding acquisition, Formal analysis, Data curation, Conceptualization. **Longwei He:** Writing – review & editing, Writing – original draft, Validation, Supervision, Project administration, Investigation, Funding acquisition, Data curation, Conceptualization. **Jia Zhou:** Validation, Resources, Methodology, Investigation, Funding acquisition, Data curation, Conceptualization.

Acknowledgments

This work was supported by The Natural Science Foundation of Hunan Province (Nos. 2022JJ30484, 2022JJ10042, 2023JJ50157), The Start-up funds of University of South China (Nos. 201RGC012, 20XQD030), The Research Foundation of Education Bureau of Hunan Province (No. 22B0418), Education Ministry's Collaborative Education Program with Industry of China (Nos. 220902102225257, 230902999244208), Ministry of Education of China: "Chunhui Plan" (No. HZKY20220359), and The Open Fund of State Key Laboratory of Chemo/Biosensing and Chemometrics (Nos. 2021013, 2021015).

Supplementary materials

Supplementary material associated with this article can be found, in the online version, at doi:10.1016/j.cclet.2024.110166.

References

[1] C. Gil-Garcia, E. Flores-Alvarez, R. Cebrian-Garcia, et al., Curr. Prob. Cardiol. 47 (2022) 101328.
[2] B. Campbell, P. Khatri, Lancet 396 (2020) 129–142.
[3] G.A. Donnan, M. Fisher, M. Macleod, et al., Lancet 371 (2008) 1612–1623.
[4] L. Lu, J. Tian, X. Luo, et al., Cell. Mol. Life Sci. 78 (2021) 63–78.
[5] S.J. Dixon, K.M. Lemberg, M.R. Lamprecht, et al., Cell 149 (2012) 1060–1072.
[6] Y. Wang, M. Lv, W. Zhao, Ageing Res. Rev. 91 (2023) 102035.
[7] W.S. Yang, R. SriRamaratnam, M.E. Welsch, et al., Cell 156 (2014) 317–331.
[8] Y. Jin, L. Ren, X. Jing, et al., Front. Pharmacol. 14 (2023) 1185071.
[9] Y. Xu, K. Li, Y. Zhao, et al., Cell. Mol. Neurobiol. 43 (2023) 205–222.
[10] I. Alim, J.T. Caulfield, Y. Chen, et al., Cell 177 (2019) 1262–1279.
[11] Y. Cui, Y. Zhang, X. Zhao, et al., Brain Behav. Immun. 93 (2021) 312–321.
[12] Y. Wang, S. Wu, Q. Li, et al., Adv. Sci. 10 (2023) e2300325.
[13] S. Yeh, C. Chen, Y. Lin, et al., Mol. Neurobiol. 60 (2023) 5902–5914.
[14] C.E. Dieteren, S.C. Gielen, L.G. Nijtmans, et al., Proc. Natl. Acad. Sci. U. S. A. 108 (2011) 8657–8662.
[15] W.H. Watson, J.C. Greenwell, Y. Zheng, et al., J. Nutr. Biochem. 84 (2020) 108431.
[16] S. Li, P. Wang, M. Ye, et al., Anal. Chem. 95 (2023) 5133–5141.
[17] M. Ali, H. Tabassum, M.M. Alam, et al., Life Sci. 293 (2022) 120338.
[18] S. Martinez De Lizarrondo, C. Gakuba, B.A. Herbig, et al., Circulation 136 (2017) 646–660.
[19] M. Khan, B. Sekhon, M. Jatana, et al., J. Neurosci. Res. 76 (2004) 519–527.
[20] Y. Zhang, R.V. Swanda, L. Nie, et al., Nat. Commun. 12 (2021) 1589.
[21] S. Li, Y. Li, H. Liu, et al., Anal. Chem. 90 (2018) 9418–9425.
[22] H. Tan, K. Zhou, J. Yan, et al., Sens. Actuat. B: Chem. 298 (2019) 126903.
[23] B. Demouveaux, V. Gouyer, F. Gottrand, et al., Adv. Colloid. Interface Sci. 252 (2018) 69–82.
[24] L. Lian, R. Zhang, S. Guo, et al., Chin. Chem. Lett. 34 (2023) 108516.
[25] L. Dai, M. Ren, W. Lin, Spectrochim. Acta. A: Mol. Biomol. Spectrosc. 254 (2021) 119627.
[26] X. Guan, J. Hong, Q. Li, et al., Sens. Actuat. B: Chem. 369 (2022) 132325.
[27] L. Chai, T. Liang, Q. An, et al., Anal. Chem. 94 (2022) 5797–5804.
[28] B.M. Coull, N. Beamer, P. de Garmo, et al., Stroke 22 (1991) 162–168.
[29] S.H. Song, J.H. Kim, J.H. Lee, et al., BMC Neurol. 17 (2017) 20.
[30] M.K. Kuimova, S.W. Botchway, A.W. Parker, et al., Nat. Chem. 1 (2009) 69–73.
[31] Y. Xu, C. Li, S. Lu, et al., Nat. Commun. 13 (2022) 2009.
[32] L. Li, Y. Huang, X. Jin, et al., Anal. Chem. 95 (2023) 17003–17010.
[33] L. Fan, Q. Yang, Q. Zan, et al., Anal. Chem. 95 (2023) 5780–5787.
[34] J. Liu, F. Meng, J. Lv, et al., Spectrochim. Acta. A: Mol. Biomol. Spectrosc. 295 (2023) 122602.
[35] Z. Wang, S. Wang, B. Wang, et al., Chem. Eng. J. 464 (2023) 142687.
[36] Y. Xu, C. Li, J. An, et al., Sci. China Chem. 66 (2023) 155–163.
[37] H. Wang, J. Wang, G. Ma, et al., Chem. Eng. J. 464 (2023) 142551.
[38] Y. Xu, W. Tuo, L. Yang, et al., Angew. Chem. Int. Ed. 61 (2022) e202110048.
[39] X. Zhang, F. Yang, T. Ren, et al., Chin. Chem. Lett. 34 (2023) 107835.
[40] F. Cheng, T. Qiang, L. Ren, et al., Analyst 146 (2021) 2632–2637.
[41] J. Zhao, Y. Qu, H. Gao, et al., Chem. Commun. 56 (2020) 1475–1478.
[42] P. Huang, W. Zhang, J. Wang, et al., Chin. Chem. Lett. 35 (2024) 109778.
[43] Y. Cheng, X. Wang, J. Chen, et al., Chin. Chem. Lett. 35 (2024) 109156.
[44] D. Chang, Y. Wang, Y. Bai, et al., Sci. Rep. 5 (2015) 16951.
[45] J. Cheng, D. Li, M. Sun, et al., Chem. Sci. 11 (2020) 281–289.
[46] J. Xiong, W. Wang, C. Wang, et al., ACS Sens. 5 (2020) 3237–3245.
[47] W. Xuan, R. Pan, Y. Wei, et al., Bioconjug. Chem. 27 (2016) 302–308.
[48] T. Liang, T. Qiang, L. Ren, et al., Chem. Sci. 13 (2022) 2992–3001.
[49] L. Shen, H. Liu, M. Jin, et al., Chin. Chem. Lett. 35 (2024) 109572.
[50] M. Agrawal, V. Kumar, M.P. Kashyap, et al., Eur. J. Pharmacol. 666 (2011) 5–11.
[51] Y. Zhu, Q. Tang, G. Wang, et al., Curr. Neurovasc. Res. 14 (2017) 132–140.
[52] G.J. Bix, E.K. Gowing, A.N. Clarkson, Transl. Stroke Res. 4 (2013) 515–523.
[53] Y.M. Kuo, Y.Y. Sun, C.Y. Kuan, J. Vis. Exp. 172 (2021) e61740.
[54] J. Hwang, N. Shin, H.J. Shin, et al., Transl. Stroke Res. 12 (2021) 866–878.
[55] B. Dong, Y. Lu, N. Zhang, et al., Anal. Chem. 91 (2019) 5513–5516.
[56] Q. Gu, Z. Yang, J. Chao, et al., Anal. Chem. 95 (2023) 12478–12486.
[57] Z. Yang, Y. He, J. Lee, et al., J. Am. Chem. Soc. 135 (2013) 9181–9185.
[58] G.O. Latunde-Dada, Biochimi. Biophys. Acta Gen. Subj. 1861 (2017) 1893–1900.
[59] I. Ingold, C. Berndt, S. Schmitt, et al., Cell 172 (2018) 409–422.
[60] R. She, D. Liu, J. Liao, et al., Front. Cell. Neurosci. 17 (2023) 1191629.
[61] J. Guo, Q.Z. Tuo, P. Lei, J. Neurochem. 165 (2023) 487–520.
[62] D. Koubi, H. Jiang, L. Zhang, et al., Neurochem. Int. 46 (2005) 73–81.
[63] M.S. Kane, A. Paris, P. Codron, et al., Biochem. Pharmacol. 148 (2018) 100–110.
[64] Y. Zhao, Y. Jiang, W. Lv, et al., J. Control. Release 233 (2016) 64–71.
[65] W. Zhang, Y. Wu, H. Chen, et al., Gene 767 (2021) 145148.
[66] A. Zhu, P. Rajendram, E. Tseng, et al., Res. Pract. Thromb. Haemost. 6 (2022) e12795.